A hybrid bioinspired catechol-alloxazine triangular nickel complex stabilizing protons and electrons

Agnideep Das, Hannah Jobelius, Jules Schleinitz, Stefani Gamboa-Ramirez, Geordie Creste, Gwendal Kervern, Jesus Raya, Nolwenn Le Breton, Aurélie Guénet, Zahia Boubegtiten-Fezoua, et al.

A hybrid bioinspired catechol-alloxazine triangular nickel complex stabilizing protons and electrons

Agnideep Das,[a] Hannah Jobelius,[a,e] Jules Schleinitz,[b] Stefani Gamboa-Ramirez,[c] Geordie Creste,[a] Gwendal Kervern,[d] Jesus Raya,[a] Nolwenn Le Breton,[a] Aurélie Guénet,[a] Zahia Boubegtiten-Fezoua,[e] Laurence Grimaud,[b] Maylis Orio,[c] Guillaume Rogez,[f] Petra Hellwig,[e] Sylvie Choua,[a] Sylvie Ferlay[e] and Marine Desage-El Murr*[a]

We report the design of a unique bioinspired ligand merging redox-active catechol and flavin-related alloxazine substructures. Upon coordination with a Ni(II) salt, this hybrid ligand forms a trinuclear complex containing three Ni^{II} centers and three redox-active ligands. This air-stable metallic triangle stabilizing protons and electrons was studied by X-ray crystallography, infra-red (IR) and UV-vis spectroscopy, SQUID magnetometry (Superconducting QUantum Interference Device), MAS-NMR (Magic Angle Spinning-Nuclear Magnetic Resonance), EPR (Electron Paramagnetic Resonance), electrochemistry and DFT (Density Functional Theory). This multidisciplinary approach supports the presence of protons located on the organic ligands, and an electronic structure involving three high spin Ni(II) ions strongly ferromagnetically coupled with radicals. Both ligand and complex provide a new design for molecular bricks and bioinspired energy storage devices.

Introduction

Flavins are essential cofactors in electron transfer proteins (flavodoxins) and oxidoreductases (flavoenzymes). A reason for their ubiquity in biological systems is their tricyclic isoalloxazine core unit which exhibits three different redox states and can overall shuttle two electrons and two protons.[1,2] A specificity of flavins is their ability to act selectively as two-electrons/two-protons or two-fold single electron/proton carriers, which is referred to as redox switching. Fine-tuning of the flavin redox activity is achieved by a combination of specific intermolecular interactions involving stacking, H-bonding, and also depends on the pH.

Radical species of known cofactors including the flavosemiquinone radical play a key role in numerous biological functions ranging from electron-transfer and hopping in proteins, small-molecule activation, signaling, biological light emission, phototropism, DNA repair, circadian clock and magnetic-field sensing.[3,4] To stabilize and harness such transient radical species, proteins use molecular strategies such as burial in hydrophobic regions,[5] and shielding of apical positions by complexation with neighboring aminoacids.[6,7] Formation of flavosemiquinone radicals can be achieved by photoexcitation and has led to synthetic applications of flavin analogues in photocatalysis.[8,9]

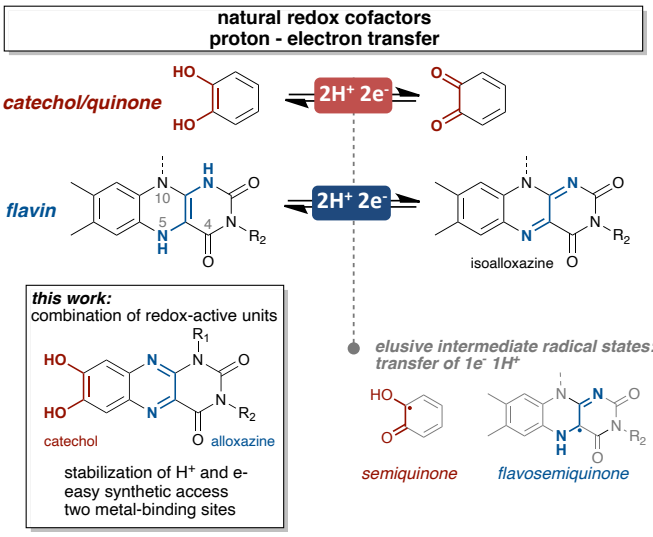

Fig. 1 Proton and electron transfers in biological redox cofactors and ligand design merging two redox-active subunits: catechol and alloxazine.

In the field of molecular materials, and especially molecular magnetism,[10] radicals have been successfully combined with metals (transition metals and/or lanthanides) to provide a new class of materials that have been intensively studied in the last decades.[11] Complexation of metal ions to flavin can also lead to the stabilization of a flavosemiquinone radical[12] and the coordination chemistry of flavin and related analogues with metals has received a great deal of attention since the early eighties.[13,14] Complexation occurs at the O^4–N^5 site between the central pyrazine core and the terminal alloxane ring[15,16] (Fig. 1) and complexes of flavins with numerous metals including copper, silver, zinc, cadmium, nickel, cobalt, iron, iridium and ruthenium have been reported.[12,15,17-25] However, while *in situ* complexation of a flavosemiquinone radical with a metal can lead to detectable signals in EPR and UV-vis absorption spectroscopies, isolation of stable metal complexes with this radical ligand has so far been elusive.

Alloxazines are structural isomers of natural flavins (isoalloxazines) in which both C=N double bonds are located within the central pyrazine ring (Fig. 1). Alloxazines present an heterocyclic 10 electron π-system and DFT calculations have shown that the radical form of alloxazine is very similar to that of isoalloxazine.[26] Alloxazines can store electrons and protons, and have recently been reported as efficient redox-active components in redox-flow batteries.[27] Complexes of alloxazine with transition metals have been reported mostly with 4d and 5d metals such as ruthenium, rhenium, iridium, tungsten, while copper was the only 3d metal investigated.[26,28-30] Although the existence of flavosemiquinone radicals is well-documented, no stable metal-flavosemiquinone complexes have been reported and especially no solid-state structures are reported in the literature for this electronic state. This is in sharp contrast with the case of catechols, a well-known class of redox-active ligands displaying three accessible redox states and which forms stable complexes with metals in their radical semiquinone state.[31] The ability of a redox-active *tris*-catechol-triphenylene ligand to stabilize electrons in extended polynuclear systems has recently been demonstrated with first-row transition metals including cobalt,[32] copper[33] and nickel.[34]

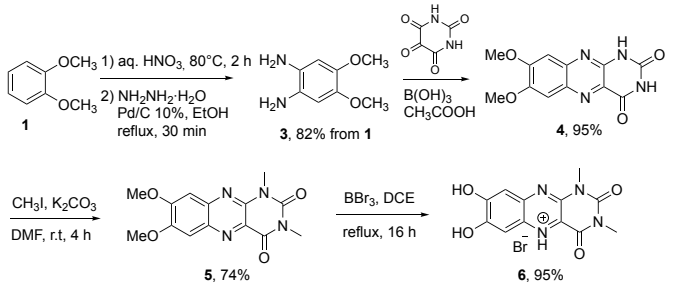

Scheme 1 Synthesis of hybrid pro-ligand.

Catechols and alloxazines share the ability to stabilize radicals when ligated to a metal, and in the case of alloxazines, protonation can occur at either nitrogen of the central pyrazine ring, thus opening the possibility of decoupling the sites for proton storage and metal complexation. Here, we report the synthesis of a hybrid ditopic ligand combining both catechol and alloxazine subunits and its complexation with nickel. An electronic structure of this unique trinuclear complex is proposed on the basis of a set of analyses and spectroscopies. This engineered ligand design allows the formation of a triangular trinuclear complex stabilizing protons and electrons, which opens the way towards the design of bioinspired energy storage molecular devices.[35,36]

Results and Discussion

Synthesis of pro-ligand and complex

The newly designed pro-ligand merging both catechol and alloxazine redox-active motifs (Fig. 1) was obtained from 1,2-dimethoxy-benzene **1** in five steps (Scheme 1 and SI). *Bis*-nitration with nitric acid followed by reduction of the nitro groups into amines with Pd/C and hydrazine yielded intermediate **3**, which was condensed with alloxane in the presence of boric acid to provide **4**, the methoxylated analogue of lumichrome (7,8-dimethylalloxazine). Methylation of the secondary amine sites of the alloxane ring was carried out using methyl iodide and the resulting compound **5** could then undergo deprotection of its methoxy groups into the free alcohol to afford **6** as a bromide salt. Complexation of **6** with nickel nitrate as metal source in the presence of triethylamine, followed by a recrystallization in N,N-dimethylformamide (DMF), as shown in scheme 2, affords **7**. Mass spectrometry (ESI-MS) of **7** shows a molecular peak at *m/z* = 992.9718, which corresponds to a $[Ni_3L_3H]^+$ ($C_{36}H_{25}N_{12}Ni_3O_{12}$) structure (see SI). **7** has very limited solubility in most solvents, and only low solubility in DMF and DMSO, which limits possible analysis in solution.

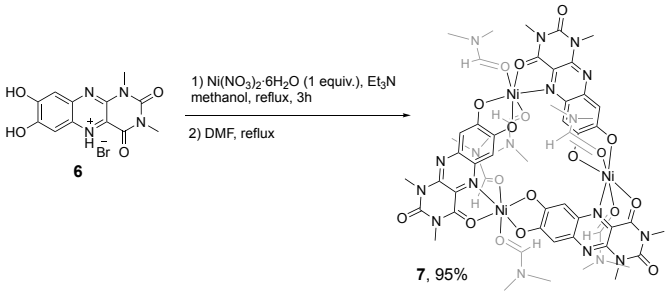

Scheme 2 Synthesis of nickel complex.

Solid state structure of 6 and 7

6 and **7** were analyzed in the solid-state by X-ray diffraction on single crystals. Slow evaporation of a solution of **6** in 1:1 CH_2Cl_2-MeOH mixture afforded orange needle-like single-crystals suitable for X-ray crystallography (see SI). The compound crystallizes in a monoclinic system, in the *P* 2_1/c space group (see table S1) and is in its cationic form $[(C_{12}H_{11}N_4O_4)^+, Br^-.CH_3OH]$. The catechol C–O distances in the aromatic benzene ring of the pro-ligand are 1.338(5) Å and 1.353(5) Å, and the corresponding C–C distance is 1.449(6) Å (Table 1). These values show that both C–O bonds display single bond character while the C–C bond has an aromatic character, which confirms that this motif is present under a catechol redox state in **6**. Regarding the two N atoms of the central pyrazine ring, both display similar C–N distances: 1.332(5) and 1.352(5) Å for one of the nitrogens and 1.327(5) and 1.360(5) Å for the other, which indicates that the cationic form of **6** displays a protonated nitrogen. As expected, **6** is completely flat and, in the crystal, strong π- π stacking between the phenyl rings of the alloxazine moieties is observed (Fig. 2) with a 3.723(10) Å distance between the phenyl rings. The bromide anions are located between the molecules and weak Br···O halogen interactions are observed with oxygen atoms from catechol moieties of two different molecules, with Br–O distances of 3.215(8) and 3.236(4) Å. A strong hydrogen bond is also observed between a MeOH solvent molecule and the protonated N atom of the alloxazine moieties, with an O–N distance of 2.660(7) Å. The other distances observed in the alloxazine core are consistent with those previously reported.[37]

Dark red prism-like single crystals of **7** suitable for X-ray crystallography were obtained by slowly cooling a supersaturated hot DMF solution (see SI). The compound crystallizes in a triclinic system, *P*-1 space group. The crystal is composed of three crystallographically independent Ni cations, three crystallographically independent ligands, and six coordinated DMF molecules. In addition, two DMF and two water molecules are present in the unit cell, and all solvents have been refined. As shown in Fig. 3a, a flat triangular trinuclear species arises through coordination between the metallic Ni cations and the ligand. This particular geometry arises from the fact that **6** was designed as a flat *bis*-bidentate ligand with a deformed L-shaped geometry that can coordinate to the metals through both catechol and alloxazine sites. This distinctive heteroleptic binding pattern results in a triangular shape for **7**. Each nickel center exhibits an octahedral geometry in which two DMF molecules act as apical ligands. Each metallic cation is in a deformed O_5N octahedral environment, as attested by distances provided in Table 1. The Ni-O values (for the catechol and the alloxazine moieties) are in accordance with an oxidation state (II) of the octahedral nickel cation. On each metallic center, both coordinated DMF ligands are in relative *trans* position, and the ligands occupy the basal positions of the coordination sphere of the metal.

In **7**, the C–O catechol bonds are in the 1.288(4)–1.300(4) Å range (Table 1), which is significantly shorter than observed in **6**, and the C–C catechol bonds are in the 1.474(4)–1.482(4) Å range, which is significantly longer than observed in **6**. These values can be compared with those reported for catechol-based complexes in all three redox states (catecholate, semiquinone SQ and benzoquinone BQ), and especially with nickel complexes which have been extensively studied from a structural point of view.[38-42] The values measured in all three ligands at the O,O site for **7** are in accordance with data reported for SQ or catecholate derivatives.[43] Concerning the three alloxazine O,N coordination sites in **7**, the C–O distances (with O coordinated to Ni) are in the 1.244(4)–1.246(4) Å range, whereas the C–N distances (with N coordinated to Ni) are in the 1.341(4)–1.354(4) Å range. These values are higher than those observed for **6**, and while there is no reported crystal structure of a metal-alloxazine complex in the semiquinone state, a useful comparison can be made considering the aminophenolate subunit (N–C–C–O) embedded in the alloxazine moiety. When compared to the values obtained for Ni(II) octahedral complexes,[44,45] the distances of this subunit in **7** are compatible with a SQ or BQ character at the N,O site (flavin) for the three ligands.[28,46] Therefore, the crystallographic data are in accordance with the presence of three Ni(II) centers and three ligands with SQ/catecholate character on the O,O centers and SQ/BQ character on the N,O binding sites (alloxazine).

It is interesting to note that the Ni2 center presents shorter distances in its first coordination sphere, compared to those of centers Ni1 and Ni3 (see table 1), suggesting a different electronic environment for this metal. Finally, distinct C–N distances at both nitrogen atoms in the central alloxazine rings (1.366(4)–1.406(4) Å range and 1.365(4)-1.398(4) Å range) suggest a possible protonation of the ligand in **7**, as observed in **6**. In addition, regarding the packing of the triangular structures in the unit cell, one can clearly observe the alternate disposition of the flat structures in the unit cell, which is also in favor of the partial protonation of the ligands (Fig. S3), but no H atoms have been placed during the refinement. In the crystal, and as shown in Fig. S3, the trinuclear units are parallelly stacked and the coordinated DMF molecules are interdigitated, with van der Waal interactions.

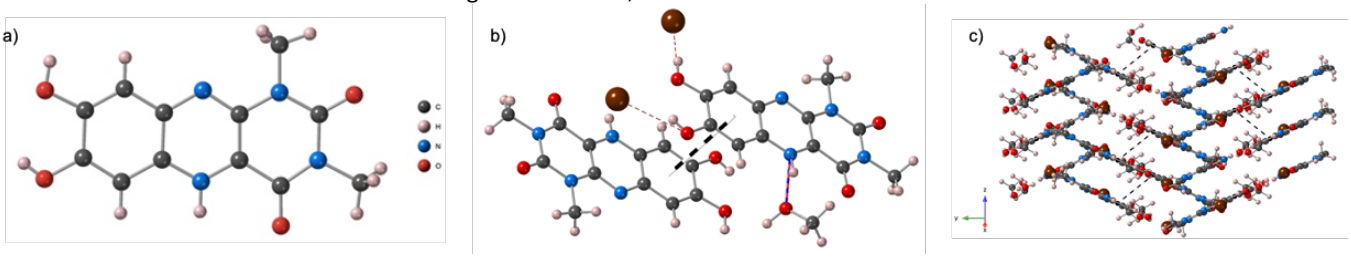

Fig. 2 Single crystal X-ray crystallography of a) pro-ligand **6**, b) supramolecular interactions involving Br-, MeOH, and π-stacking interactions, and c) packing of the ligands in the unit cell.

	C-$O_{catechol}$ (Å)	C-$C_{catechol}$ (Å)	C-O_{allox} (Å)	C-$N_{allox\ central\ ring}$ (Å)	C_{ring}-$N_{allox\ methyl}$ (Å)	Ni-O (Å)	Ni-N_{allox} (Å)	Ni-O_{DMF} (Å)
Pro-ligand **6**	1.338 (5) 1.353 (5)	1.449(6)	1.214 (5) 1.222 (5)	1.327(5) + 1.360(5) 1.332(5) +1.352(5)	1.377(5) + 1.381(5) 1.374(5) + 1.400(5)	-	-	-
Metal complex **7**	1.288(4) 1.295(4) 1.297(4) 1.299(4) 1.300(4)	1.474(4) 1.475(4) 1.482(4)	Free 1.215(4) 1.216(4) 1.225(4) Coordinated 1.244(4) 1.245(4) 1.246(4)	Free 1.331(4) + 1.363(4) 1.326(4) + 1.366(4) 1.331(4) + 1.360(4) Coordinated 1.341(4) + 1.348(4) 1.344(4) + 1.345(4) 1.342(4) + 1.354(4)	1.366(4) + 1.402(4) 1.376(4) + 1.393(4) 1.371(4) + 1.406(4) 1.365(4) + 1.398(4) 1.369(4) + 1.401(4) 1.377(4) + 1.395(4)	Catechol 1.969(2) Ni2 1.971(2) Ni3 1.978 (2) Ni1 2.059(2) Ni2 2.069(2) Ni1 2.076(2) Ni3 Allox 2.081(2) Ni2 2.106(2) Ni3 2.110(2) Ni1	2.111 (3) 2.114(3) 2.141 (2)	2.070(2) 2.075(2) 2.077(2) 2.094(2) 2.096(2) 2.109(2)

Table 1 Relevant distances for **6** and **7**.

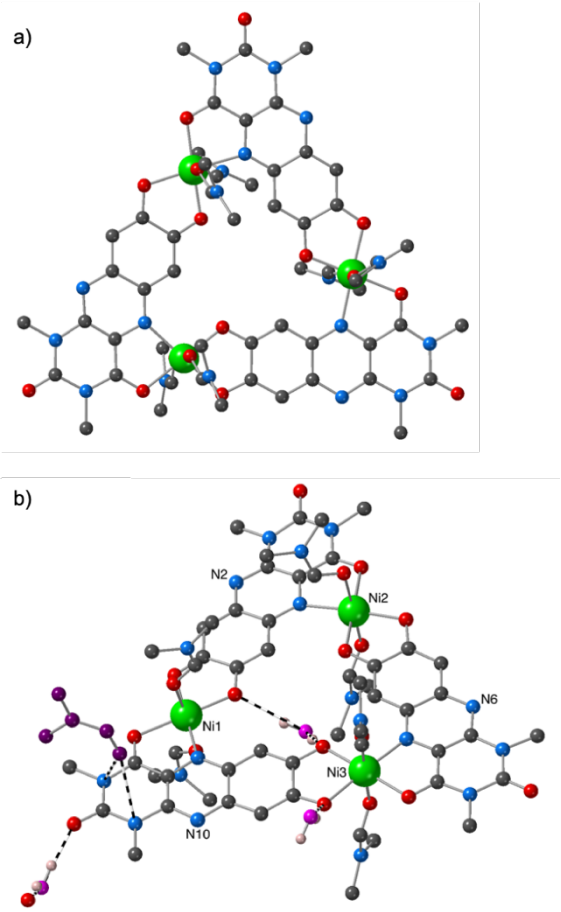

Fig. 3 Structural drawing of **7** showing a) the planar triangular complex and b) the supramolecular interactions observed in **7**: pink atoms represent oxygen atoms of water molecules and non coordinated DMF is depicted in violet. H atoms omitted except those involved in H-bonding.

A closer inspection of the crystal structure reveals the presence of supramolecular interactions. The free solvents slightly interact with the trinuclear species: there are strong hydrogen bonds between a free water molecule and O atoms from the alloxazine motif, with O–O distances of 2.794(5) Å and 2.937(6) Å. The formed triangle appears as an isosceles triangle, with Ni-Ni distances of 7.486(6), 7.487(6) and 7.539(6) Å. Four molecules of free solvents (two DMF and two H_2O) are present in the unit cell, and some of them are slightly interacting with the trinuclear species. There are strong hydrogen bonds between free water molecules and O atoms from SQ/catecholate moieties, with O–O distances of 2.794(5) Å and 3.223(6) Å, and also an interaction between a water molecule and an O atom of the alloxazine moieties with O–O distances of 2.937(5) Å, as shown in Fig. 3b and Fig. S4). In addition, a molecule of DMF is strongly interacting with the alloxazine ring with O–N distances of 3.121(5) and 3.182(5) respectively (Fig. 3b). These supramolecular interactions are breaking the C_{3v} symmetry within the triangle, and as shown in Fig. 3b, Ni1 and Ni3 present a different environment than that of Ni2. When exposed to air, compound **7** is clearly hygroscopic, as attested by elemental analysis, which is in rather good agreement with the presence of 8.5 water molecules in the unit cell. The TGA measurements (see SI, Fig. S5) show that the mass loss begins at ambient conditions. The decrease in mass of 23% between RT and 150°C is consistent with the presence of two lattice DMF molecules and around 10 water molecules. The coordinated DMF molecules are released above 150°C.

Electrochemical properties of 6 and 7 in solution

To gain insight into the redox behaviors of **6** and **7**, electrochemical studies were carried out. The cyclic voltammetry of **6** in DMSO (dimethylsulfoxide) performed towards oxidation potentials displays a single oxidation peak detected at + 0.93 V, which accounts for the oxidation of both bromide and catechol moieties (Fig. 4a). Towards reduction potentials, several reduction waves can be detected for **6** but the first reduction occurs at $E_{1/2}$ = -0.36 V in DMSO (Fig. 1b). By analogy with reduction of flavin mononucleotide[47,48] the latter could be attributed to the reduction of the protonated iminium in **6**. Indeed, addition of 1 equiv of triethylamine shifted the reduction wave to more cathodic potentials ($E_{1/2}$ = -0.88 V in DMSO, Fig. 4b).[47] This value is also consistent with the first reduction potential detected for methoxylated intermediate **5** (Scheme 1, $E_{1/2}$ = -1.05 V in DMSO) (Fig. S13).

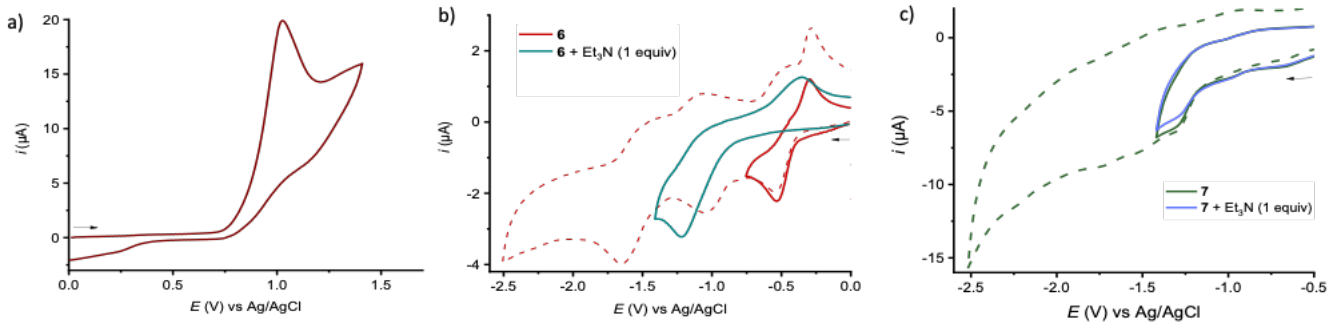

Fig. 4 Cyclic voltammetry of a 2 mM solution of **6** in DMSO with 0.1 M of Bu_4NBF_4 at rt at a scan rate of 0.2 V s-1 towards a) oxidation and b) reduction potentials; c) cyclic voltammetry of a 2 mM solution of **7** in DMSO with 0.1 M of Bu_4NBF_4 towards reduction potentials at 50 °C at a scan rate of 0.2 V s-1 on a 1 mm GC electrode.

Due to solubility issues, the cyclic voltammetry of **7** was performed in DMSO at 50 °C and a first reduction peak at -1.32 V was observed, corresponding to an irreversible electron transfer (Fig. 4c, green curve, for more detailed CV studies see SI). No difference was observed after addition of 1 equiv of base on **7** (Fig. 4c, blue curve). This lack of modification and the value of this reduction peak suggest that this first reduction wave could be attributed to the reduction of Ni(II) centers as concluded by Clarke for riboflavin-ligated ruthenium complexes.[49]

UV-Vis studies in solution

(Iso)-alloxazines display strong absorption bands in UV-Vis spectroscopy and this technique can offer interesting insights regarding the presence of ligand-based radicals in such systems. Hemmerich and co-workers have studied the complexation of flavins with several first-row d-block metals, among which nickel.[17,18] The authors observed a red shift in the UV-vis spectra and ascribed it to a Ni-flavin complex although no further characterization was reported. The absorption properties of **6** and **7** were studied in DMSO solutions. The UV-vis spectrum of **6** displays two characteristic bands at 366 nm and 399 nm (Fig. 5a). These absorption bands may be attributed to spin-allowed pro-ligand-centered transitions involving both the alloxazine and catechol parts of the ligand. However, and as previously reported, the absorption spectrum of 1,3-dimethyllumichrome, a closely related alloxazine derivative, is insensitive to pH variation (pH range from 3 to 11) and absorption spectroscopy cannot therefore be used to probe protonation state of the N atoms at positions 5 or 10.[50] Upon complexation, the 400 nm band is red-shifted to 452 nm. This value is close to that reported for a Ni^{II}–flavosemiquinone complex (460 nm), which the authors assigned to the flavosemiquinone state of the ligand by comparison to the UV-vis spectrum of free flavin radical (477 nm).[18] Based on the literature for alloxazine metal complexes, the new band at 452 nm could be attributed to metal-to-ligand charge transfer (MLCT (metal-to-ligand charge transfer), d_π to π^*) transitions arising from metal complexation at the O^4-N^5 sites. These transitions have been reported at 470 and 564 nm for the reduction of metal-flavobenzoquinone (M-FlavBQ) complexes into metal-flavosemiquinone (M-FlavSQ, M = Cu and Ru respectively).[26] It is worth mentioning that while the ε (molar absorption coefficient) value of the 452 nm band is relatively high for a MLCT transition, **7** bears three flavosemiquinone-type ligands unlike the complexes reported, where only one is present. All these observations support the presence of flavosemiquinone radicals in **7** in DMSO solution.

Oxidation of **7** was carried out by addition of increasing amounts of ferrocenium (Fc^+, PF_6^-) in DMSO and was monitored by UV-vis spectroscopy (Fig. 5b). It should be noted that the absorption bands of ferrocenium and ferrocene appear respectively at 621, 443, 326 and 260 nm in DMSO.[51] The presence of two isosbestic points evidences the clean conversion of **7** into a single species upon oxidation. The characteristic band at 452 nm disappears concomitantly with the appearance of a new band at 420 nm and two other large bands appear between 500 and 700 nm (530 and 650 nm). Based on previous work evidencing the possibility of ligand-centered redox processes,[26] this new band (655 nm) may be attributed to intervalence charge transfer (IVCT) transitions and suggests the presence, in solution, of ligand-based radicals in this new species. This observation points towards a conversion into a single species containing mixed-charge ligands and exhibiting IVCT transitions. Behavior of **7** upon reduction with $CoCp_2$ was also studied but did not lead to appreciable changes in the UV-vis profile (Fig. S21).

Solution and solid-state IR spectroscopy

IR spectroscopy can provide detailed information on the electronic and coordination environments by probing selected vibrational modes within the molecular structure. ATR-FTIR (Attenuated Total Reflection - Fourier-transform infrared spectroscopy) spectra were recorded for **6** and **7** samples both as powder and as dried film from a solution in DMSO. The data obtained for the powder are shown in the supplementary information (See Fig. S22 and Table S2). At 1673 and 1718 cm^{-1}, two stretching (C=O) vibrational modes are seen for the pro-ligand. Upon coordination to nickel, an important shift of these two bands toward lower wavenumbers (1591 and 1670 cm^{-1}, respectively) is observed with an increase in the intensity of the band at 1591 cm^{-1}. A similar behavior was observed for the two stretching (C=N) vibrational modes when comparing the data obtained for the pro-ligand and the complex. The shifts observed here for the C=O and the C=N groups reflect the coordination of the ligand to the metal ion through these functional groups, and also the structural reorganization of the ligand. The different bands obtained for the ligand were tentatively assigned to vibrational modes attributed previously to similar alloxazine derivatives and catechol structures. [28,52-54] All contributions and their tentative assignments for **6** and **7** are summarized in table S2.

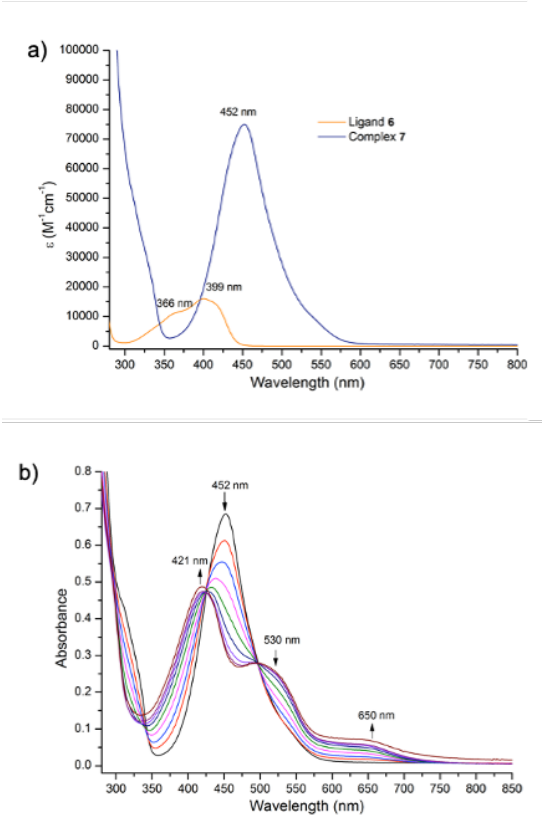

Fig. 5 a) Comparison of UV spectra of **6** and **7** in DMSO; b) UV-Vis titration of oxidation of **7** with ferrocenium in degassed DMSO (rt, 10^{-5} mol L^{-1}) by one equivalent increments.

In order to confirm these tentative assignments and to identify (de)protonable or hydrogen-bond forming groups in **7**, hydrogen deuterium exchange experiments ($^1H/^2H$ exchange) were performed. $^1H/^2H$ exchange is frequently used in IR spectroscopy to reflect solvent accessibility and the hydrogen bonding environment in complex molecules like proteins,[55-57] but it may also be used to identify exchangeable residues in organic molecules. The experimental procedure used here is detailed in the SI section. The ATR-FTIR spectrum obtained for **7** in the presence of ^2H_2O displays the main features already observed in the presence of ^1H_2O (See Fig.6, inset of Fig. S23 in the region from 1400 to 800 cm^{-1}), with small shifts in positions that can be attributed to the exchange. The absorption bands tentatively attributed to the ν(N-C-N), δ(O-H) and the ring mode of **7** shift in both position and intensity (See Fig.6 and Table S3). Concomitant small variations of the δ(N-H) and δ(C-H) modes at 952 and 1117 cm^{-1} respectively are also seen. These changes confirm that exchangeable protons are present in **7**, suggesting a certain protonation degree of this species. The shifts are around 2-5 cm^{-1}. Such rather small changes are typically observed in the case of coupling of the vibrational modes to neighboring groups, and can be expected for ring vibrations or in the presence of resonance structures.

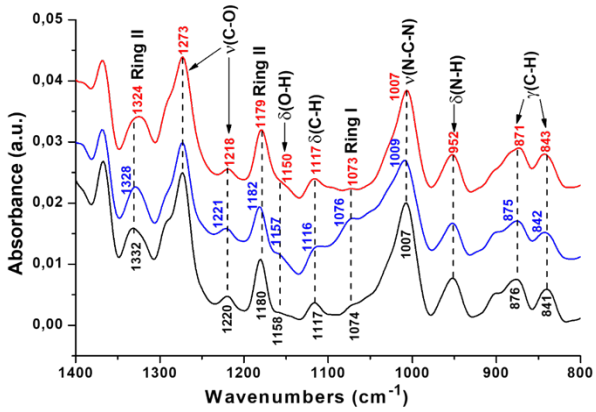

Fig. 6 ATR-FTIR spectra of **7** as dry films from solutions in DMSO (black curve), in DMSO in the presence of H_2O (blue curve) and in DMSO in the presence of D_2O (red curve). The DMSO solvent was interactively subtracted from each spectrum. This figure is the inset of the figure S23 on the region from 1400 to 800 cm^{-1}.

Solid-state ultra-fast MAS ^1H NMR spectroscopy

We next turned our attention towards solid-state spectroscopic techniques and magnetic measurements. Several direct 1D proton solid-state NMR spectroscopy experiments were performed at 17.75 T, under 50 kHz magic angle spinning (ultra-fast MAS) and variable temperature. Three signals were observed and their isotropic shifts, chemical shift anisotropies (CSA) and line-shape were fitted using the DMFit program.[58] Each isotropic shift showed variability upon temperature variation. Given the chemical environment of the 25 protons and the overall symmetry of the structure, we propose the following assignment for the three proton shifts: -0.2 ppm for the methyl groups (N-CH_3), 8.3 ppm for the aromatic protons (Ar-H) and 32.0 ppm for the protons on the nitrogen atoms (NH) (Fig. 7, S24-S25). The abnormal shifts (*ca* 30 ppm) and CSA (*ca* 150 ppm) for protons, as well as their temperature dependence are expected for paramagnetic species, for which the hyperfine interaction is bound to dominate the chemical shift interactions. This hyperfine interaction is carried by two

possible media: through molecular orbitals (Fermi-contact shift) or through space (pseudo-contact shift or dipolar).[59] In solid-state NMR spectroscopy, both dipolar and contact contributions will have an effect on the CSA, but their contribution to isotropic shifts can be variable.

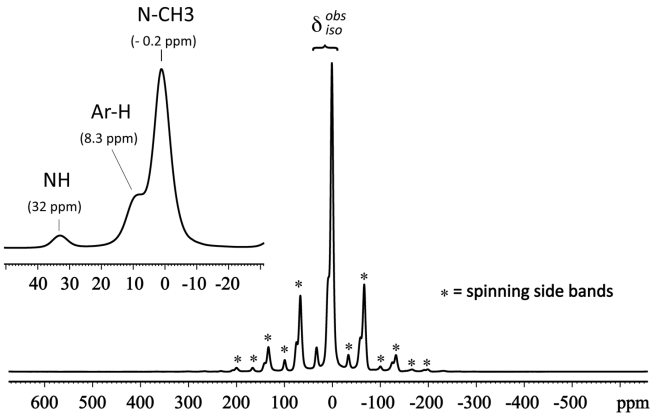

Fig. 7 Solid state ^{1}H NMR spectrum of **7** obtained at high field (750.12MHz) and an ultra-fast Magic Angle Spinning (MAS) rate of 50kHz. Inset: expansion of the isotropic chemical shift zone with the proposed assignments.

In order to determine the hyperfine coupling constant for each signal, the temperature-dependent isotropic shifts were plotted versus the temperature dependent molecular magnetic susceptibility inferred from magnetic measurements (Fig. S26). Given the behavior of each NMR signal versus temperature variation, we deduce that for each signal there is only one hyperfine coupling constant. Consequently, each signal proceeds from ensembles of very similar chemical environments, and the dipolar component being proportional to $1/r^3$ (where r is the electron-nucleus distance), it does not disrupt the pseudo-equivalence imposed by chemical environment and local symmetries and therefore can be considered as having a negligible effect on the isotropic shifts. We deduce from this study an ensemble of diamagnetic shifts and hyperfine coupling constants for each signal, with a proposed assignment (Table S4). The diamagnetic shift for the aromatic protons is somehow unusual and could arise from π-stacking interactions in which these protons could be shielded by a neighboring aromatic ring in the crystal structure.

Solid-state EPR spectroscopy measurements

Redox-active ligands are known to promote interligand coupling through metal centers and ligand-based redox activity, which can generate mixed-charge species[60] and the study of their electronic properties by EPR spectroscopy is thus of strong relevance. Metal complexation to the flavin N,O binding site has been documented over the past few decades.[12,17,19,21,22] While spectroscopic evidence showing that 3d metals can bind to the flavosemiquinone redox state was obtained by several spectroscopies including UV-vis, EPR , and IR, there is however, and as already mentioned, no reported X-ray structure of a Ni-flavin or metal-flavosemiquinone complex. Hemmerich *et al.* reported an EPR spectroscopic study evidencing a Zn-radical chelate in a flavo-coenzyme system.[61] Similar studies using Ni(II) and Fe(II) metal precursors did not provide clear spectroscopic evidence for a flavosemiquinone radical, which was attributed to spin-spin interaction between Ni and the radical ligand system.[62] The Q-band EPR spectra of the crystal powder of **7** at room temperature exhibits two components, one of which is a very broad line (Fig. 8a). The effective *g* values respectively at 3.6 and 2.1 could be attributed to a high spin species with a zero-field splitting larger than the microwave quantum. When the temperature decreases to 4 K, the intensity of the various components decreases, which indicates an antiferromagnetic behavior in line with SQUID measurements (see below). Q-band EPR spectra of the amorphous powder of nickel complex before recrystallization, therefore without apical DMF molecules, were recorded in order to compare to the crystal powder **7** (Fig. 8b). At room temperature, only one transition at g = 2.001 is observed, consistently with ligand-based SQ radical(s) and square planar Ni(II) (S=0).

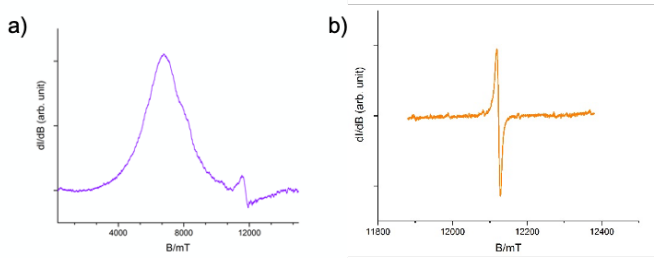

Fig. 8 Room temperature Q-band EPR spectrum of a) crystal powder of **7**: 100 kHz modulation frequency, microwave power of 2.4 mW, sweep width 1600 mT, modulation amplitude 0.4 mT, sweep time 600 s; b) amorphous powder of **7**: 100 kHz modulation frequency, microwave power of 2.4 mW, sweep width 50 mT, modulation amplitude 0.4 mT, sweep time 120 s.

SQUID measurements

Further investigations on the magnetic state of **7** were carried out by SQUID measurements (Fig. 9). The temperature dependence of the magnetic susceptibility χ and of the χT product of **7** were investigated in the 1.8–300 K temperature range with an applied field of 5 kOe. The χT product remains essentially constant from room temperature (5.7 emu·K·mol^{-1}) to *ca.* 100 K when it starts decreasing regularly down to 1.8 K (2.2 emu·K·mol^{-1}). The $1/\chi$ = f(T) can be modelled in the high temperature region (above 150 K) using the Curie–Weiss law, providing C = 5.71(1) emu·K·mol^{-1} and a negative Weiss temperature θ= -0.02(1) K, which indicates the occurrence of weak antiferromagnetic interactions (Fig. S27), as suggested by EPR spectroscopy measurements.

To account for the value of the Curie constant, the almost constant χT product between 100 and 300 K, the fact that the system is EPR-silent (in X-band) and the presence of protons and radicals on the ligand discussed above, various hypotheses can be considered for the magnetic description of the system. First of all, it is worth underlining that the magnetic data is incompatible with the absence of radicals (expected maximum Curie constant C = 4.0 emu K mol^{-1} for three Ni(II) ions with g = 2.3) or with the presence of only one radical per formula unit (expected maximum Curie constant C = 4.3 emu·K·mol^{-1} for three Ni(II) ions (S = 1) with g = 2.3 and one weakly coupled radical with g = 2.0, or C = 5.1 emu·K·mol^{-1} considering two Ni(II)

ions (S = 1) with g = 2.3 and one radical strongly ferromagnetically coupled with one Ni(II) ion (leading to a S = 3/2 ground spin state, with excited S = 1/2 spin state not populated at room temperature) with g = 2.3).

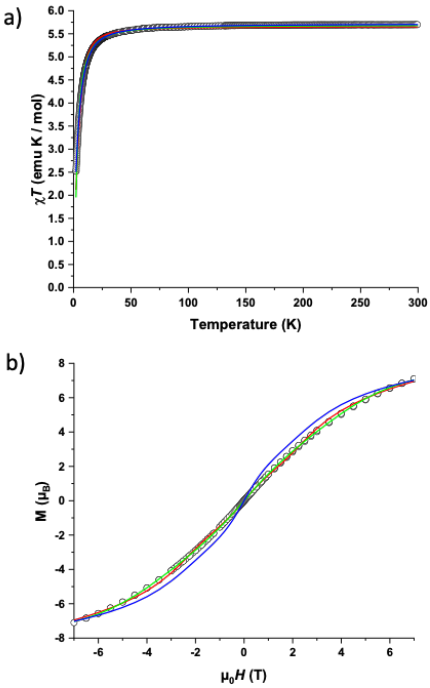

Fig. 9 a) χT product *vs.* T for the title compound under an applied *dc* field of 0.5 kOe; b) M *vs.* T at 1.8 K. Open symbols: experimental points, full red lines: best fit considering an equilateral triangle of spins S = 3/2, full green lines: best fit considering an isosceles triangle of two spins S = 1 and one spin S = 2 and full blue lines: best fit considering an isosceles triangle of one spin S = 1 and two spins S = 3/2 (see text).

The first reasonable hypothesis is to consider as paramagnetic species three Ni(II) ions (S = 1) and three SQ$^{\bullet}$ radicals (S = 1/2), each Ni(II) ion being very strongly ferromagnetically coupled to one SQ$^{\bullet}$ radical. This $J_{Ni\text{-}SQ}$ ferromagnetic coupling has to be stronger than *ca.* 150 cm^{-1}, so that no significant population of the excited spin doublet state can be observed at room temperature, which is also consistent with EPR spectroscopy measurements of the crystals (In all the manuscript, including for DFT studies (see below), the magnetic interaction constants J are reported with respect to the $-2J\ S_1 \cdot S_2$ spin coupling Hamiltonian). This is in line with what has been observed for other Ni-SQ systems.[63] With these assumptions, the system can be satisfactorily described as a triangle of spin S = 3/2, which corresponds to a theoretical Curie constant of 5.63 emu·K·mol^{-1} considering g = 2. The fit of the magnetic behavior was performed simultaneously on M = f(H) and χT = f(T).[64] To avoid overparameterization, we chose an equilateral triangle topology. Considering the crystallographic evidences of small deviations from a perfect C_3 symmetry, it is much likely that this spin-frustration configuration is in fact cancelled. Nevertheless, taking into account more than one intramolecular exchange interaction, rhombicity, or more than one set of parameters (g and D) for the Ni-Rad formal entities, does not significantly improves the fit. The fit leads to $g_{Ni\text{-}SQ}$ = 2.01(1), $J_{(Ni\text{-}SQ)\text{-}(Ni\text{-}SQ)}$ = --0.24(2) cm^{-1} and $|D_{Ni\text{-}SQ}|$ = 5.8(1) cm^{-1}.

A second hypothesis consists in considering an isosceles triangle spin topology constituted by three Ni(II) ions (S = 1), one of them being very strongly ferromagnetically coupled to two SQ$^{\bullet}$ radicals. This topology allows to take into account the slightly different coordination environment around the Ni2 center, as shown by XRD analysis. As for the previous hypothesis, the $J_{Ni\text{-}SQ1\bullet}$ and $J_{Ni\text{-}SQ2\bullet}$ ferromagnetic coupling exchange constants have to be stronger than *ca.* 150 cm^{-1}, so that no significant population of the excited spin states can be observed at room temperature. With these assumptions, the system can be satisfactorily described as a triangle of two S = 1 spins (corresponding to the spin states of the two basal Ni(II) ions) and one S = 2 spin (corresponding to the ground spin-state of the summit SQ$^{\bullet}$-Ni-SQ$^{\bullet}$ entity), which corresponds to a theoretical Curie constant of 5.51 emu·K·mol^{-1} considering g = 2.1. The fit of the magnetic behaviour, performed simultaneously on χT = f(T) and M = f(H) leads to $g_{(SQ\bullet\text{-}Ni\text{-}SQ\bullet)}$ = 2.22(1), g_{Ni} = 2.01(1), $J_{Ni\text{-}Ni}$ = -1.95(2) cm^{-1} and $|D_{(SQ\bullet\text{-}Ni\text{-}SQ\bullet)}|$ = 7.33(2) cm^{-1}. The values obtained for $|D_{Ni}|$ (axial anisotropy parameter for the two basal Ni(II) ions) and $J_{Ni\text{-}(SQ\bullet\text{-}Ni\text{-}SQ\bullet)}$ (exchange coupling value between the SQ$^{\bullet}$-Ni-SQ$^{\bullet}$ formal entity and the Ni(II) ions) are negligible in this approach, but very strongly dependent on the starting values chosen. Therefore, to avoid useless overparameterization, these parameters were constrained to zero during the fit.

Finally, a third and last hypothesis consists in considering once more three Ni(II) ions and two radicals, but without constraining the two radicals to interact with the same Ni(II) ion as for the previous one, and instead choosing a coupling scheme where each radical interacts with a different Ni(II) ion. There again, the coupling between a Ni(II) ion and a radical has to be strongly ferromagnetic. The system can thus be described as a triangle of one S = 1 spin (corresponding to the spin state of a single Ni(II) ion) and two S = 3/2 spin (corresponding to the ground spin-state of the basal Ni-SQ$^{\bullet}$ entities), which corresponds to a theoretical Curie constant of 5.24 emu·K·mol^{-1}considering g = 2.1. Unfortunately, it has not been possible to obtain a satisfying fit with this topology. The best fit leads to $g_{(Ni\text{-}SQ\bullet)}$ = 2.17(1), g_{Ni} = 2.29(1), $J_{Ni\text{-}(Ni\text{-}SQ\bullet)}$ = -0.35(1) cm^{-1}, $|D_{(Ni\text{-}SQ\bullet)}|$ = 7.11(2) cm^{-1} and $|D_{Ni}|$ = 5.20(3) cm^{-1}. The exchange coupling value between the two (Ni-SQ$^{\bullet}$) formal entities was found to be negligible and thus constrained to zero during the fit. The χT = f(T) curve is perfectly reproduced, even better than with the two previous hypotheses, but the M = f(H) is not, despite the use of already numerous parameters. There again, rhombicity might be taken into account, but the number of parameters would make the fit irrelevant.

DFT

To further support our assumptions on the electronic structure of **7**, as well as the protonation state of the ligand and the presence of ligand-based radicals, DFT calculations were performed on the trinuclear complex. Three configurations were considered, all of them containing three high-spin Ni(II) ions. The first model features three protons and three ligand-

based radicals, the second model displays two protons and two ligand-based radicals, and the third set of models combines only one proton and one ligand-based radical. These model systems were all subjected to geometry optimizations and their Gibbs free energies were calculated. Based on energetic considerations (Table S4), the models with 1 proton and 1 electron are too high in energy compared to the other configurations and will not be considered any longer. The model considering three protons and three radicals appears as the most stable one but a fully protonated state of the ligand is not supported by XRD and HRMS data. The second most stable model with two protons and two radicals remains the only one able to describe the electronic structure of **7** (Fig. S28).

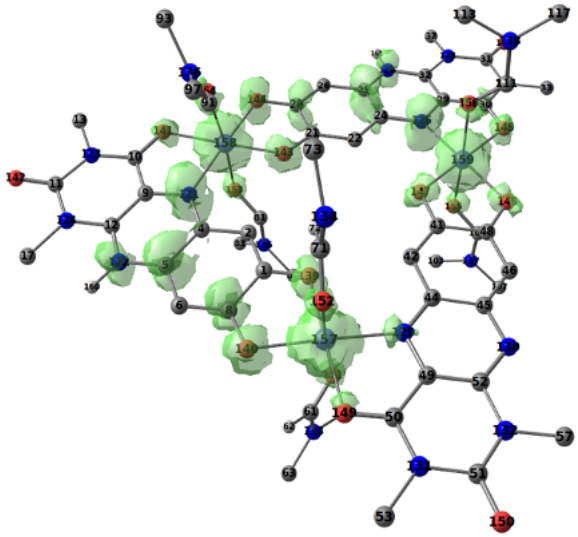

Fig. 10 Spin density plot of **7** considering 3 HS (high-spin) Ni(II) centers, two SQ-radicals and two protons on the ligand. Remaining hydrogen atoms were removed for clarity.

Looking first at the spin density distribution, we observe that two SQ-radicals are delocalized in the vicinity of Ni2 (Table S5 and Fig. 10) which allows to describe the triangle as a system of three high spin Ni(II) ions (S = 1) with one of them interacting with two SQ-radicals (SQ$^{\bullet}$-Ni-SQ$^{\bullet}$). In order to probe the magnetic interaction between the Ni center and the SQ-radical as well as the one between the Ni ions, two small model systems were built (Fig. S30-S33, Tables S6-S7). Using the "broken symmetry"[65,66] (BS) approach within the density functional theory (DFT) framework, we were able to calculate $J_{Ni\text{-}SQ}$ = 131 cm^{-1} (model A) and $J_{Ni\text{-}Ni}$ = 15 cm^{-1} (model B) for the two types of interactions (Fig. S34-S36, Tables S8-S9). The results are in fair agreement with the experimental values obtained from SQUID measurements and further support that **7** can be described as a triangle with two protons on the ligand and three high-spin Ni(II) ions combined to two ligand-based radicals.

Discussion

The ditopic pro-ligand bearing two redox-active subunits and the triangular complex have been structurally characterized in the solid state, and their protonation and electronic state were studied by a combination of solution and solid-state spectroscopies together with DFT calculations. The presence of protonated ligand(s) in **7** is unambiguously supported by XRD, IR and MAS-NMR spectroscopies while the presence of ligand-based radicals is confirmed by combined XRD, UV-vis and EPR spectroscopies. Further determination of the degree of protonation and radical stabilization by SQUID and DFT studies leads to a set of possible models. All these models imply the presence of three Ni(II) centers (S=1), with strong ferromagnetic coupling between nickel centers and ligand-based radicals, and encompass the following possible protonation/radical ligand schemes: 3H$^+$/3e$^-$ and 2H$^+$/2e$^-$. The 1H$^+$/1e$^-$ state is supported neither by SQUID nor by DFT and can thus be ruled out. Furthermore, the clean conversion upon oxidation into a single species exhibiting IVCT (intervalence charge transfer) transitions strongly supports the presence of at least two ligand-based radicals in **7**. A full 3H$^+$/3e$^-$ state is supported by SQUID and DFT but is not fully coherent with the XRD and HRMS analyses. Meanwhile, the 2H$^+$/2e$^-$ state is also compatible with XRD and DFT studies, although it leads to unperfect fits for SQUID measurements, considering two possibilities: the two radicals as strongly ferromagnetically coupled to either one Ni center, or free to interact with two vicinal Ni centers.

Interestingly, while all models focusing on the localization of the protons and electrons on the metal complex itself do not allow a definitive picture to emerge, it should be noted that XRD studies clearly show the presence of supramolecular and stacking interactions along with the fact that all Ni centers are not equivalent. This lower degree of symmetry and solid-state interactions imply that the possibility that a proton could be shared between two molecules of **7** in the lattice, and therefore not fully assigned to a single triangle unit, should be considered but cannot be explicitly modelled. Also, the possibility that several configurations could coexist is in accordance with the high planarity of the system, where delocalization of the electrons can easily occur. The particular design of the flat ditopic redox-active pro-ligand and its association with nickel cations lead to a flat triangular complex with a well-defined molecular structure but an extended and highly delocalized electronic structure and protonation scheme.

Conclusion

We report the design of a hybrid bioinspired ligand merging catechol and alloxazine structural units, which forms a new class of redox-active ligand stabilizing electrons and protons. The pro-ligand has been characterized in solution and in the solid-state, evidencing a protonated species. Upon combination with a nickel salt, a unique triangular trinuclear species was obtained, and characterized both in solution and solid state. Its electronic structure has been studied by a multidisciplinary approach combining several techniques. The presence of protons and ligand-based radicals was unambiguously established, as well as the presence of Ni(II) centers strongly ferromagnetically coupled with these radicals. The distinctive features of this flat ditopic ligand combining a catechol subunit

to an alloxazine core have several consequences on the electronic structure and protonation state of the metal complex including enhanced electronic delocalization over the structure and stabilization of protons shared between several molecules in the lattice by stacking and supramolecular interactions. Although the remarkable ability of flavins to stabilize radicals is largely due to delocalization on the diazine central ring and flanking aromatic ring,[67] this work shows that introduction of a catechol moiety does not compromise electron delocalization while leveraging metal coordination properties. The combination of such unique ligand involving multisite redox groups with metallic species can build a new class of molecular materials such as redox-active coordination polymers or networks for efficient electronic transfer.

Author contributions

AD carried out synthetic work, characterization, data collection and wrote the experimental section. HJ carried out synthetic work, performed and analyzed the IR studies, and wrote the experimental section. JS performed cyclic voltammetry studies, analyzed the data and wrote the experimental section. SGR carried out DFT studies and analyzed the data. GC carried out synthetic work and analyzed the data. GK and JR collected and analyzed the MAS-NMR data, and contributed to the manuscript. NLB collected and analyzed the EPR data, and contributed to the manuscript. AG analyzed the X-Ray and UV-Vis data, and contributed to the manuscript. ZBF collected and analyzed the IR data, and contributed to the manuscript. LG supervised the electrochemistry studies, analyzed the data, contributed to the manuscript and discussions. MO supervised the DFT studies, analyzed the data, and contributed to the manuscript and discussions. GR performed and analyzed the SQUID data, and contributed to the manuscript and discussions. PH supervised and analyzed the IR data, and contributed to the manuscript and discussions. SC supervised and analyzed the EPR data, and contributed to the manuscript and discussions. SF performed, supervised and analyzed the TGA and X-ray data analysis, and contributed to the manuscript and discussions. MDEM designed the study, supervised the experiments, analyzed the data and wrote the manuscript with input from all co-authors.

Conflicts of interest

There are no conflicts to declare.

Acknowledgements

This work has benefited from support by the initiative of Excellence IDEX-Unistra (ANR-10-IDEX-0002-02) from the French national program “Investment for the Future”, Agence Nationale pour la Recherche (ANR-20-CE05-0005-01, ANR-18-CE092-0040-01), CNRS and Université de Strasbourg. The authors also acknowledge Labex NIE (ANR-11-LABX-0058_NIE within the Investissement d'Avenir program) for the support to the magnetometry platform. The authors thank Chaima Hammami and Daria Torodii for assistance in solid-state MAS NMR experiments. We are grateful to NMR, mass spectrometry and X-ray diffraction common services (Dr. Lydia Karmazin) from Federation de Chimie “Le Bel” – FR 2010 and FrenchBIC network.

Notes and references

Crystal structures of **6** and **7** have been deposited in the Cambridge Crystallographic Database CCDC under the references CCDC 2089518 (**6**) and CCDC 2089519 (**7**).

1 F. Müller, *Chemistry and biochemistry of flavoenzymes*, CRC Press, 1991.
2 *Flavins: Photochemistry and Photobiology*, RSC Publishing, Eds. E. Silva and A. M. Edwards., 2006.
3 K. S. Conrad, C. C. Manahan and B. R. Crane, Photochemistry of flavoprotein light sensors, *Nat. Chem. Biol.*, 2014, **10**, 801–809.
4 P. Müller and M. Ahmad, Light-activated Cryptochrome Reacts with Molecular Oxygen to Form a Flavin–Superoxide Radical Pair Consistent with Magnetoreception, *J. Biol. Chem.*, 2011, **286**, 21033–21040.
5 G. Ulas, T. Lemmin, Y. Wu, G. T. Gassner and W. F. DeGrado, Designed metalloprotein stabilizes a semiquinone radical, *Nat. Chem.*, 2016, **8**, 354–359.
6 Z. T. Campbell and T. O. Baldwin, Two Lysine Residues in the Bacterial Luciferase Mobile Loop Stabilize Reaction Intermediates, *J. Biol. Chem.*, 2009, **284**, 32827–32834.
7 Z. T. Campbell, A. Weichsel, W. R. Montfort and T. O. Baldwin, Crystal Structure of the Bacterial Luciferase/Flavin Complex Provides Insight into the Function of the β Subunit, *Biochemistry*, 2009, **48**, 6085–6094.
8 B. König, S. Kümmel and R. Cibulka, in *Chemical Photocatalysis*, De Gruyter, Berlin, Boston, 2013.
9 A. Graml, T. Neveselý, R. Jan Kutta, R. Cibulka and B. König, Deazaflavin reductive photocatalysis involves excited semiquinone radicals, *Nat. Commun.*, 2020, **11**, 3174.
10 E. Coronado, Molecular magnetism: from chemical design to spin control in molecules, materials and devices, *Nat. Rev. Mater.*, 2020, **5**, 87–104.
11 P. Turek, Organic Radicals and Molecular Magnetism in *Electron Paramagnetic Resonance Spectroscopy: Applications*, ed. P. Bertrand, Springer International Publishing, Cham, 2020, pp. 247–282.
12 L. E. Göran Eriksson, Magnetic properties of some flavin metal complexes, *Biochim. Biophys. Acta (BBA) - General Subjects*, 1970, **208**, 528–531.
13 W. Kaim, B. Schwederski, O. Heilmann and F. M. Hornung, Coordination compounds of pteridine, alloxazine and flavin ligands: structures and properties, *Coord. Chem. Rev.*, 1999, **182**, 323–342.
14 W. Kaim and B. Schwederski, Non-innocent ligands in bioinorganic chemistry—An overview, *Coord. Chem. Rev.*, 2010, **254**, 1580–1588.
15 C. J. Fritchie, The Structure of a Metal-Flavin Complex 10-methylisoalloxazine silver nitrate, *J. Biol. Chem.*, 1972, **247**, 7459–7464.

16 S. Fukuzumi and T. Kojima, Control of redox reactivity of flavin and pterin coenzymes by metal ion coordination and hydrogen bonding, *J. Biol. Inorg. Chem.*, 2008, **13**, 321–333.

17 A. Ehrenberg, P. Hemmerich, M. Nilsson, A. Melera and L. Nilsson, The Near IR Absorption of Metal Complexes with Flavin Free Radicals, *Acta Chem. Scand.*, 1964, **18**, 1320–1321.

18 F. Müller, P. Hemmerich and A. Ehrenberg, Light Absorption of Flavosemiquinone Metal Chelates, *Eur. J. Biochem.*, 1968, **5**, 158–164.

19 J. Lauterwein, P. Hemmerich and J. M. Lhoste, Flavoquinone-metal complexes. I. Structure and properties, *Inorg. Chem.*, 1975, **14**, 2152–2161.

20 J. Lauterwein, P. Hemmerich and J. M. Lhoste, Flavoquinone-metal complexes. II. Paramagnetic interactions, *Inorg. Chem.*, 1975, **14**, 2161–2168.

21 M. Goodgame and K. W. Johns, Metal complexes of flavin mononucleotide, *Inorg. Chim. Acta*, 1979, **37**, L559–L560.

22 M. Goodgame and K. W. Johns, Spectral studies of some complexes of riboflavin-2′,3′,4′,5′-tetraacetate, *Inorg. Chim. Acta*, 1979, **34**, 1–4.

23 M. Benecky, T.-J. Yu, K. L. Watters and J. T. McFarland, Metal-flavin complexation. A resonance Raman investigation, *Biochim. Biophys. Acta (BBA) - Protein Structure*, 1980, **626**, 197–207.

24 M. G. Dowling and M. J. Clarke, Electrochemistry of metalloflavin complexes in dimethylformamide, *Inorg. Chim. Acta*, 1983, **78**, 153–160.

25 B. Schwederski and W. Kaim, Complexes of folic acid, lumiflavin and riboflavin with bis(2, 2′-bipyridine)ruthenium(II). Facilitated formation of flavosemiquinone complexes and substantial decrease of pKa(NH), *Inorg. Chim. Acta*, 1992, **195**, 123–126.

26 F. M. Hornung, O. Heilmann, W. Kaim, S. Zalis and J. Fiedler, Metal vs Ligand Reduction in Complexes of 1,3-Dimethylalloxazine (DMA) with Copper(I), Ruthenium(II), and Tungsten(VI). Crystal Structures of (DMA)WO_2Cl_2 and (Bis(1-methylimidazol-2-yl)ketone)WO_2Cl_2, *Inorg. Chem.*, 2000, **39**, 4052–4058.

27 K. Lin, R. Gómez-Bombarelli, E. S. Beh, L. Tong, Q. Chen, A. Valle, A. Aspuru-Guzik, M. J. Aziz and R. G. Gordon, A redox-flow battery with an alloxazine-based organic electrolyte, *Nat. Energy*, 2016, **1**, 16102.

28 O. Heilmann, F. M. Hornung, J. Fiedler and W. Kaim, Organometallic iridium(III) and rhenium(I) complexes with lumazine, alloxazine and pterin derivatives, *J. Organomet. Chem.*, 1999, **589**, 2–10.

29 Y. Inui, M. Shiro, T. Kusukawa, S. Fukuzumi and T. Kojima, A triangular prismatic hexanuclear iridium(III) complex bridged by flavin analogues showing reversible redox processes, *Dalton Trans.*, 2013, **42**, 2773–2778.

30 P. Mondal, R. Ray, A. Das and G. K. Lahiri, Revelation of Varying Bonding Motif of Alloxazine, a Flavin Analogue, in Selected Ruthenium(II/III) Frameworks, *Inorg. Chem.*, 2015, **54**, 3012–3021.

31 C. G. Pierpont and R. M. Buchanan, Transition metal complexes of o-benzoquinone, o-semiquinone, and catecholate ligands, *Coord. Chem. Rev.*, 1981, **38**, 45–87.

32 Y. Suenaga, H. Inada, M. Inomata, R. Yamaguchi, T. Okubo, M. Maekawa and T. Kuroda-Sowa, Crystal Structure and Characterization of Trinuclear Cobalt(III) Complex with 2,3,6,7,10,11-Hexahydroxytriphenylene, *Chem. Lett.*, 2014, **43**, 562–564.

33 L. Yang, X. He and M. Dincă, Triphenylene-Bridged Trinuclear Complexes of Cu: Models for Spin Interactions in Two-Dimensional Electrically Conductive Metal–Organic Frameworks, *J. Am. Chem. Soc.*, 2019, **141**, 10475–10480.

34 Y. Wang, F. Lambert, E. Rivière, R. Guillot, C. Herrero, A. Tissot, Z. Halime and T. Mallah, Electronic and spin delocalization in a switchable trinuclear triphenylene trisemiquinone bridged Ni3 complex, *Chem. Commun.*, 2019, **55**, 12336–12339.

35 M. Desage-El Murr, Nature is the Cure: Engineering Natural Redox Cofactors for Biomimetic and Bioinspired Catalysis, *ChemCatChem*, 2020, **12**, 53–62.

36 A. Das, C. Hessin, Y. Ren and M. Desage-El Murr, Biological concepts for catalysis and reactivity: empowering bioinspiration, *Chem. Soc. Rev.*, 2020, **49**, 8840-8867.

37 A. Ertan and J. Koziol, Structure of 1,3,9-trimethylalloxazine, *Acta Cryst. Section C*, 1993, **49**, 2179–2181.

38 A. V. Piskunov, G. K. Fukin, Yu. A. Kurskii, V. K. Cherkasov and G. A. Abakumov, The interaction of nickelocene with 3,6-di-tert-butyl-o-benzoquinone, *Inorg. Chem. Commun.*, 2005, **8**, 339–342.

39 C. Brückner, D. L. Caulder and K. N. Raymond, Preparation and Structural Characterization of Nickel(II) Catecholates, *Inorg. Chem.*, 1998, **37**, 6759–6764.

40 M. P. Bubnov, I. A. Teplova, N. O. Druzhkov, G. K. Fukin, A. V. Cherkasova and V. K. Cherkasov, Catecholato complexes of cobalt and nickel with 1,4-disubstituted-1,4-diazabutadiens-1,3 and 1,2-bis(diphenylphosphino)ethane, *J. Chem. Sci.*, 2015, **127**, 527–535.

41 H. Yang, Y. Zhao, B. Liu, J.-H. Su, I. L. Fedushkin, B. Wu and X.-J. Yang, Noninnocent ligands: heteroleptic nickel complexes with α-diimine and 1,2-diketone derivatives, *Dalton Trans.*, 2017, **46**, 7857–7865.

42 L. A. Cameron, J. W. Ziller and A. F. Heyduk, Near-IR absorbing donor–acceptor ligand-to-ligand charge-transfer complexes of nickel(II), *Chem. Sci.*, 2016, **7**, 1807–1814.

43 S. N. Brown, Metrical Oxidation States of 2-Amidophenoxide and Catecholate Ligands: Structural Signatures of Metal–Ligand π Bonding in Potentially Noninnocent Ligands, *Inorg. Chem.*, 2012, **51**, 1251–1260.

44 S. Ghorai and C. Mukherjee, Effect of ligand substituent on the reactivity of Ni(II) complexes towards oxygen, *Dalton Trans.*, 2014, **43**, 394–397.

45 A. Ali, D. Dhar, S. K. Barman, F. Lloret and R. Mukherjee, Nickel(II) Complex of a Hexadentate Ligand with Two o-Iminosemiquinonato(1−) π-Radical Units and Its Monocation and Dication, *Inorg. Chem.*, 2016, **55**, 5759–5771.

46 R. Mukherjee, Assigning Ligand Redox Levels in Complexes of 2-Aminophenolates: Structural Signatures, *Inorg. Chem.*, 2020, **59**, 12961–12977.

47 S. L. J. Tan, J. M. Kan and R. D. Webster, Differences in Proton-Coupled Electron-Transfer Reactions of Flavin Mononucleotide (FMN) and Flavin Adenine Dinucleotide (FAD) between Buffered and Unbuffered Aqueous Solutions, *J. Phys. Chem. B*, 2013, **117**, 13755–13766.

48 S. L. J. Tan and R. D. Webster, Electrochemically Induced Chemically Reversible Proton-Coupled Electron Transfer Reactions of Riboflavin (Vitamin B2), *J. Am. Chem. Soc.*, 2012, **134**, 5954–5964.

49 M. J. Clarke and M. G. Dowling, Cyclic voltammetry studies of metalloflavin complexes in aqueous solution, *Inorg. Chem.*, 1981, **20**, 3506–3514.

50 D. Prukała, E. Sikorska, J. Koput, I. Khmelinskii, J. Karolczak, M. Gierszewski and M. Sikorski, Acid–Base Equilibriums of Lumichrome and its 1-Methyl, 3-Methyl, and 1,3-Dimethyl Derivatives, *J. Phys. Chem. A*, 2012, **116**, 7474–7490.

51 U. M. Rabie, Intra- and intermolecular charge transfer: Twin themes and simultaneous competing transitions involving ferrocenes, *Spectrochim. Acta Part A: Molecular and Biomolecular Spectroscopy*, 2009, **74**, 746–752.

52 M. Abe, Y. Kyogoku and T. Kitagawa, lnfrared spectra and molecular association of lumiflavin and riboflavin derivatives, *Spectrochim. Acta Part A: Molecular Spectroscopy*, 1986, **42**, 1059–1068.

53 S. Griffith and W. Greaves, Vibrational spectra of catechol, catechol-d2 and -d6 and the catecholate monoanion, *Spectrochim. Acta Part A: Molecular Spectroscopy*, 1991, **47**, 133–140.

54 R. Foglizzo and A. Novak, Infrared and Raman Spectra of Pyrazinium Halides, *Appl. Spectrosc., AS*, 1970, **24**, 601–605.

55 C. Vigano, M. Smeyers, V. Raussens, F. Scheirlinckx, J. M. Ruysschaert and E. Goormaghtigh, Hydrogen-deuterium exchange in membrane proteins monitored by IR spectroscopy: A new tool to resolve protein structure and dynamics, *Biopolymers*, 2004, **74**, 19–26.

56 K. S. Kim, J. A. Fuchs and C. K. Woodward, Hydrogen exchange identifies native-state motional domains important in protein folding, *Biochemistry*, 1993, **32**, 9600–9608.

57 Y. Neehaul, S. Kriegel, B. Barquera and P. Hellwig, Functional Studies on Membrane Proteins by Means of H/D Exchange in Infrared: Structural Changes in Na^+ NQR from *V. cholerae* in the Presence of Lipids. In: Lacapere JJ. (eds) Membrane Protein Structure and Function Characterization. Methods in Molecular Biology, vol 1635. Humana Press, New York, NY, 2017, 247–257.

58 D. Massiot, F. Fayon, M. Capron, I. King, S. L. Calvé, B. Alonso, J.-O. Durand, B. Bujoli, Z. Gan and G. Hoatson, Modelling one- and two-dimensional solid-state NMR spectra, *Magnetic Resonance in Chemistry*, 2002, **40**, 70–76.

59 I. Bertini, C. Luchinat, G. Parigi and E. Ravera, *Solution NMR of Paramagnetic Molecules*, Elsevier, 2017.

60 C. G. Pierpont, Ligand Redox Activity and Mixed Valency in First-Row Transition-Metal Complexes Containing Tetrachlorocatecholate and Radical Tetrachlorosemiquinonate Ligands, *Inorg. Chem.*, 2011, **50**, 9766–9772.

61 P. Hemmerich, D. V. Dervartanian, C. Veeger and J. D. W. Van Voorst, Evidence from electron-spin-resonance spectra for metal chelation shifting flavin-leucoflavin equilibria towards radical state, *Biochim. Biophys. Acta*, 1963, **77**, 504–506.

62 P. Hemmerich, D. V. Dervartanian, C. Veeger and J. D. W. Van Voorst, Evidence from electron-spin-resonance spectra for metal chelation shifting flavin-leucoflavin equilibria towards radical state, *Biochim. Biophys. Acta*, 1963, **77**, 504–506.

63 C. Benelli, A. Dei, D. Gatteschi and L. Pardi, Synthesis, redox behavior, magnetic properties, and crystal structure of a nickel(II)-semiquinone adduct with an unusually strong ferromagnetic coupling, *Inorg. Chem.*, 1988, **27**, 2831–2836.

64 N. F. Chilton, R. P. Anderson, L. D. Turner, A. Soncini and K. S. Murray, PHI: A powerful new program for the analysis of anisotropic monomeric and exchange-coupled polynuclear d- and f-block complexes, *J. Comput. Chem.* 2013, **34**, 1164–1175.

65 L. Noodleman, Valence bond description of antiferromagnetic coupling in transition metal dimers, *J. Chem. Phys.*, 1981, **74**, 5737–5743.

66 L. Noodleman and D. A. Case, Density-Functional Theory of Spin Polarization and Spin Coupling in Iron—Sulfur Clusters in *Advances in Inorganic Chemistry*, ed. R. Cammack, Academic Press, 1992, vol. 38, pp. 423–470.

67 H.-D. Hausen, A. Schulz and W. Kaim, Flavosemiquinone model systems. Part 3. Molecular and crystal structure of the cation radical salt 1,4,6,7-tetramethylquinoxalinium triiodide, *J. Chem. Soc., Perkin Trans. 2*, 1993, 343–345.